

# Maximum Likelihood Time Synchronization for Zero-padded OFDM

Koosha Pourtahmasi Roshandeh, *Student Member, IEEE*, Mostafa Mohammadkarimi, *Member, IEEE*, and Masoud Ardakani, *Senior Member, IEEE*

**Abstract**—Existing Orthogonal Frequency-Division Multiplexing (OFDM) variants based on cyclic prefix (CP) allow for efficient time synchronization, but suffer from lower power efficiency compared to zero-padded (ZP)-OFDM. Because of its power efficiency, ZP-OFDM is considered as an appealing solution for the emerging low-power wireless systems. However, in the absence of CP, time synchronization in ZP-OFDM is a very challenging task. In this paper, the non-data-aided (NDA) maximum-likelihood (ML) time synchronization for ZP-OFDM is analytically derived. We show that the optimal NDA-ML synchronization algorithm offers a high lock-in probability and can be efficiently implemented using Monte Carlo sampling (MCS) technique in combination with golden-section search. To obtain the optimal NDA-ML time synchronization algorithm, we first derive a closed-form expression for the joint probability density function (PDF) of the received ZP-OFDM samples in frequency-selective fading channels. The derived expression is valid for doubly-selective fading channels with mobile users as well. The performance of the proposed synchronization algorithm is evaluated under various practical settings through simulation experiments. It is shown that the proposed optimal NDA-ML synchronization algorithm and its MCS implementation substantially outperforms existing algorithms in terms of lock-in probability.

**Keywords**—Time-synchronization, ZP-OFDM, timing offset (TO), non-data-aided, maximum-likelihood (ML), Monte Carlo sampling.

## I. INTRODUCTION

Orthogonal frequency-division multiplexing (OFDM) modulation is a widely used technique for transmission over mobile wireless channels since it offers high spectral efficiency whilst providing resilience to frequency-selective fading [1]. One of the key requirements for optimum demodulation of OFDM signals is accurate time synchronization because a small synchronization error can dramatically degrade the system performance. Hence, a variety of time synchronization methods have been developed for OFDM systems [2]–[7]. These methods typically consist of two tasks: 1) offset estimation, and 2) offset correction. The former task relies on statistical signal processing algorithms to obtain an estimation of timing offset (TO) incurred due to lack of common time

reference between the transmitter and receiver [8]–[10]. The latter task is a simple compensation of TO by shifting [6].

Time synchronization for OFDM can be performed using either synchronization-assisting signals, such as pilot signals and synchronization symbols [11], or exploiting some redundant information in the transmitted signal, such as the guard interval redundancy employed to combat the inter symbol interference (ISI) in frequency-selective fading channels. The former approach is data-aided (DA), and the latter is non-data-aided (NDA) time synchronization [12]. DA time synchronization comes at the cost of reduced spectral efficiency, especially for short burst transmission, which is widely employed in Internet of Things (IoT) use case of the fifth generation (5G) wireless systems [13].

Guard intervals are useful for time synchronization in OFDM systems [14]. The guard interval can be in the form of cyclic prefix (CP) [15]–[17], zero-padded (ZP) [18]–[20], and known symbol padding (KSP) [21]. The choice of ZP versus CP and KSP depends on several parameters, such as the operating signal-to-noise ratio (SNR), delay spread of the fading channel, and coherent versus differential demodulation. ZP-OFDM provides great benefits over CP-OFDM and KSP-OFDM in the sense that [22] 1) it guarantees symbol recovery regardless of the channel zero locations; hence, it can improve the BER, 2) it enables finite impulse response equalization of channels regardless of the channel nulls, 3) it makes channel estimation and channel tracking easier compared to that of CP-OFDM, and 4) it offers higher power efficiency.

While DA time synchronization for ZP-OFDM has been well explored in the literature [12], NDA approach has not been extensively investigated. Hence, the focus of this work is on NDA time synchronization for ZP-OFDM.

### A. Related Work

For ZP-OFDM, most existing DA approaches rely on periodic autocorrelation properties of the received signal induced by the employed training sequences with good autocorrelation properties [23]. Moreover, most of the DA approaches developed for CP-OFDM can be applied to ZP-OFDM [24]–[27]. On the other hand, to the best of the authors' knowledge, the few existing NDA synchronization approaches for ZP-OFDM have been developed based on change point detection methods [28] or cyclostationarity properties in OFDM signal [29]. Synchronization algorithms based on change point detection usually employ a transition metric, tracing the ratio of power in two slicing windows corresponding to each TO hypothesis in the OFDM packet. These NDA solutions do

K. P. Roshandeh and M. Ardakani are with the Faculty of Electrical and Computer Engineering, University of Alberta, Edmonton, AB T6G 2R3, Canada (e-mail: pourtahm@ualberta.ca; ardakani@ualberta.ca).

M. Mohammadkarimi is with the Department of Electrical and Computer Engineering, The University of British Columbia, Vancouver, BC, V6T 1Z4, Canada, (e-mail: mmkarimi@ece.ubc.ca)

not always offer a good performance in terms of lock-in probability, i.e. correct synchronization. Moreover, we show that their performance further drops in doubly-selective (time- and frequency-selective) fading channels.

### B. Motivation

In the presence of perfect time synchronization, ZP-OFDM offers higher reliability and power efficiency compared to CP-OFDM [22]. Hence, ZP-OFDM can be considered an appealing solution for low-power IoT networks. One of the main reasons that ZP-OFDM has not been extensively used in practice is attributed to the lack of an efficient time synchronization method. While sub-optimal CP-based synchronization algorithms in CP-OFDM offer high lock-in probabilities, there is no synchronization algorithm with comparable performance for ZP-OFDM [12]. In addition, derivation of the optimal maximum likelihood (ML) time synchronization for ZP-OFDM, which results in a high lock-in probability, has remained intact. This is mainly because there currently exist no compact expression for the joint probability density function (PDF) of the received samples. Moreover, most existing synchronization methods ignore time-selectivity of the fading channel, i.e., the devastating effect of mobility and Doppler spread on time synchronization.

Motivated by the advantages of ZP-OFDM for the emerging low-power wireless networks, we study the problem of NDA-ML time synchronization for ZP-OFDM. In the first step, and for the first time, we derive a closed-form expression for the PDF of the received ZP-OFDM samples in frequency-selective fading channel. We then use the PDF of the samples to approximate their joint PDF. The joint PDF is given to a hypothesis testing algorithm to find the TO. Simulation results show that the proposed NDA-ML time synchronization algorithm significantly outperforms other existing NDA time synchronization methods. For example, at 5 dB  $E_b/N_0$  for WiMAX SUI-4 channels [28], the proposed NDA-ML time synchronization algorithm achieves a lock-in probability of 0.85 while the state of the art [28] achieves 0.55.

### C. Contributions

The main contributions of this paper are as follows:

- A closed-form approximate expression for the joint PDF of the received ZP-OFDM samples in frequency-selective fading channels is derived.
- The NDA-ML time synchronization for ZP-OFDM in frequency-selective fading channels is analytically derived. The proposed method exhibits the following advantages: (i) unlike existing sub-optimal NDA time synchronization methods, it is applicable to highly selective fading channels, such as the ones in underwater communications and ultra wideband (UWB) communication, (ii) it is valid for doubly-selective fading channels, and (iii) it can be used for both frame and symbol synchronization.
- A low-complexity implementation of the developed theoretical NDA-ML time synchronization algorithm by using Monte Carlo sampling (MCS) technique and golden-section search is proposed.

- Complexity analysis of the proposed time synchronization methods is provided.

The remaining of the paper is organized as follows: Section II introduces the system model. Section III describes the derivation of the NDA-ML time synchronization. In Section IV, a practical implementation of the proposed time synchronization algorithm by employing MCS technique and golden-section search is presented. Simulation results are provided in Section V, and conclusions are drawn in Section VI.

*Notations:* Throughout this paper, we use bold lowercase and bold uppercase letters to show column vectors and matrices, respectively. The symbols  $(\cdot)^*$ ,  $(\cdot)^{\{rmT\}}$ ,  $|\cdot|$ , and  $\lfloor \cdot \rfloor$  denote conjugate, transpose, absolute value, and floor function, respectively.  $\mathbb{E}\{\cdot\}$  denotes the statistical expectation, and  $\Re\{\cdot\}$  and  $\Im\{\cdot\}$  represent the real and imaginary parts, respectively. The subscripts I and Q show the in-phase and quadrature components of a variable. The symbols  $\cap$  and  $\cup$  denote the set intersection and union operands, respectively.

## II. SYSTEM MODEL

We consider a ZP-OFDM system in frequency-selective fading channel. Let  $\{x_{n,k}\}_{k=0}^{n_x-1}$ ,  $\mathbb{E}\{|x_{n,k}|^2\} = \sigma_x^2$ , be the  $n_x$  complex data to be transmitted in the  $n$ -th OFDM symbol. The OFDM modulated baseband signal is given by [30], [31]

$$x_n(t) = \sum_{k=0}^{n_x-1} x_{n,k} e^{j2\pi kt/T_x}, \quad 0 \leq t \leq T_x, \quad (1)$$

where  $T_x$  and  $W \triangleq n_x/T_x$  is the OFDM symbol duration and channel bandwidth, respectively. To avoid ISI, zero-padding guard interval of length  $T_z$  is added to each OFDM symbol. Hence,  $x_n(t)$  is extended into  $s_n(t)$  as

$$s_n(t) = \begin{cases} x_n(t) & 0 \leq t < T_x \\ 0 & T_x \leq t < T_x + T_z. \end{cases} \quad (2)$$

The OFDM signal in (2) propagates through a multi-path fading channel with the equivalent baseband impulse response as follows

$$h(\tau) = \sum_i \alpha_i \delta(\tau - \tau_i), \quad (3)$$

where  $\alpha_i \in \mathbb{C}$ . The delay spread of the channel in the ensemble sense is  $\tau_d$  where  $\mathbb{E}\{|\alpha_i|^2\} = 0$  for  $\tau_i > \tau_d$ .

When the transmitter and receiver are synchronized and there is no ISI, i.e.  $T_z \geq \tau_d$ , the complex baseband received signal sampled at multiples of  $T_{sa} \triangleq 1/W$  is given by

$$y_n[k] = \sum_{l=0}^{n_h-1} h[n n_s + k; l] s_n[k - l] + w_n[k], \quad (4)$$

$m = 0, 1, \dots, n_s - 1$ , where  $n_s = \lfloor (T_x + T_z)/T_{sa} \rfloor$ ,  $s_n[m] \triangleq s_n(m T_{sa})$ ,

$$h[l] = \sum_i \alpha_i g[l - \tau_i W], \quad (5)$$

$l = 0, 1, \dots, n_h - 1$ ,  $n_h \triangleq \lfloor \tau_d / T_{sa} \rfloor$ ,  $g[l] \triangleq g(lT_{sa})$ ,  $g(t) \triangleq g_{Tx}(t) \otimes g_{Rx}(r)$  with  $g_{Tx}(t)$  and  $g_{Rx}(t)$  as transmit and receive filters, respectively. Also,  $w_n[m] \sim \mathcal{CN}(0, \sigma_w^2)$  is the additive white Gaussian noise (AWGN).

We consider the wide-sense stationary uncorrelated scattering (WSSUS) assumption so that the channel coefficients from different delay taps are independent. The channel taps  $h[l]$ ,  $l = 0, 1, \dots, n_h - 1$ , are modeled as statistically independent zero-mean complex Gaussian random variables (Rayleigh fading) with the delay profile

$$\mathbb{E}\{h[l]h^*[l-m]\} = \sigma_{h_l}^2 \delta[m], \quad (6)$$

$l = 0, 1, \dots, n_h - 1$ , where

$$\sigma_{h_l}^2 = \mathbb{E}\{|h[l]|^2\} = \sum_i \mathbb{E}\{|\alpha_i|^2\} |g[l - \tau_i W]|^2. \quad (7)$$

It is assumed that the delay profile of the fading channel is known to the receiver.

*Remark 1:* The PDP of an environment is obtained through field measurements by transmitting a short pulse (wide-band) and measuring the received power as a function of delay at various locations in a small area during channel sounding. These measurements are then averaged over spatial locations to generate a profile of the average received signal power as a function of delay. [32]. Theoretically, the PDP is defined as the expectation of the squared impulse response of the channel as

$$\check{p}(\tau) = \mathbb{E}\{|h(\tau)|^2\}. \quad (8)$$

Assuming WSSUS scattering, the PDP is given as

$$\check{p}(\tau) = \sum_{k=0}^N \alpha_k \delta(\tau - \tau_k). \quad (9)$$

To determine the number of paths  $N$ , different criteria for model order selection are available in the existing literature. Estimating the path delays using frequency domain pilots is equivalent to estimating the arrival angle using an antenna array [33]. Hence, well-known signal processing techniques, e.g., estimation of signal parameters via rotational invariance techniques (ESPRIT) [34], can be adopted for this purpose. With the estimates of path delays, the path gains  $\alpha_k$ ,  $k = 0, 1, \dots, N$ , can be obtained using typical linear estimators [35].

We define  $n_z \triangleq \lfloor T_z / T_{sa} \rfloor$  as the number of padded zeros. Hence, the number of samples per ZP-OFDM symbol is  $n_s \triangleq n_x + n_z$ . Equation (4) can be written in a vector form as follows

$$\mathbf{y}_n = \begin{cases} \mathbf{H}\mathbf{s}_n + \mathbf{w}_n \triangleq \mathbf{v}_n + \mathbf{w}_n, & n \geq 0 \\ \mathbf{w}_n, & n < 0, \end{cases} \quad (10)$$

where

$$\mathbf{s}_n \triangleq \begin{bmatrix} s_n[0] \\ s_n[1] \\ \vdots \\ s_n[n_s - 1] \end{bmatrix} = \begin{pmatrix} x_n(0) \\ \vdots \\ x_n((n_x - 1)T_{sa}) \\ 0 \\ \vdots \\ 0 \end{pmatrix} \left\{ \begin{array}{l} n_x \\ n_z \end{array} \right\}, \quad (11)$$

$$\mathbf{y}_n \triangleq [y_n[0] \ y_n[1] \ \dots \ y_n[n_s - 1]]^T, \quad (12a)$$

$$\mathbf{w}_n \triangleq [w_n[0] \ w_n[1] \ \dots \ w_n[n_s - 1]]^T, \quad (12b)$$

$$\mathbf{v}_n \triangleq [v_n[0] \ v_n[1] \ \dots \ v_n[n_s - 1]]^T, \quad (12c)$$

$\mathbf{H}$  is an  $n_s \times n_s$  matrix, where its  $i$ -th ( $0 \leq i \leq n_s - 1$ ) column is  $[\mathbf{0}_{i-1} \ h[nn_s + i - 1; 0] \ h[nn_s + i - 1; 1] \ \dots \ h[nn_s + i - 1; n_h - 1] \ \mathbf{0}_{n_s - n_h - i + 1}]^T$ ,  $\mathbf{v}_n \triangleq \mathbf{H}\mathbf{s}_n$ , and  $\mathbf{w}_n$  is the AWGN vector.

Based on the Central Limit Theorem (CLT), the  $T_{sa}$ -spaced baseband OFDM samples can be accurately modeled by independent and identically distributed (i.i.d) zero-mean complex Gaussian random variables as follows [36]

$$x_n(mT_{sa}) \sim \mathcal{CN}(0, \sigma_x^2), \quad (13)$$

where

$$\mathbb{E}\{x_n(mT_{sa})x_n^*(kT_{sa})\} = \sigma_x^2 \delta[m - k]. \quad (14)$$

We consider that the transmitter and receiver are not synchronized in time domain, and there is a TO between them defined as  $\tau \triangleq dT_{sa} + \epsilon$ , where  $d$  and  $\epsilon$  represent the integer and fractional part of the TO. The fractional part of the delay appears as phase offset at each sub-carrier. Hence, its effect is compensated when carrier frequency offset is estimated [6]. However, estimation of the integer part  $d$  is required in order to detect the starting point of the fast Fourier transform (FFT) at the receiver. Estimating the integer part of the TO is the subject of this paper. We consider that the transmitter does not use pilot or preamble for TO estimation; thus, the receiver relies on the received samples, noise samples in the zero-guard interval, and the second-order statistics of the fading channel to estimate the TO.

### III. MAXIMUM LIKELIHOOD ESTIMATION

In this section, we analytically derive the NDA-ML TO estimator for ZP-OFDM. For the ease of discussions and presentation, we consider  $d \in \{-n_s + 1, \dots, -1, 0, 1, \dots, n_s - 1\}$ . However, the range of  $d$  can be considered arbitrary large.

We first formulate TO estimation as a multiple hypothesis testing problem as  $H_p : d = p$  where  $-n_s + 1 \leq p \leq n_s - 1$ . Since both positive and negative values of TO are considered, the ML estimator can address frame and OFDM symbol synchronization. Considering negative TO enables us to find the onset of the packet and incorporating positive TO enables us to

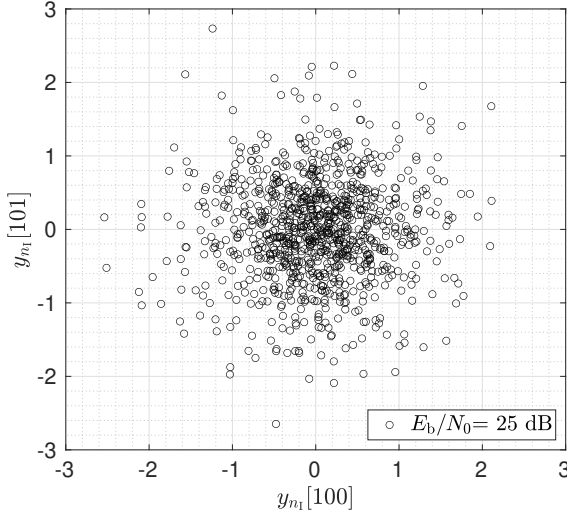


Fig. 1: Scatter plot of  $y_{10I}[100]$  and  $y_{10I}[101]$  given hypothesis  $H_0$  at 25 dB  $E_b/N_0$  ( $n_x = 128, n_z = 15, n_h = 10, n = 10$ ).

find the starting point of the ZP-OFDM symbols to efficiently apply FFT for channel equalization and data detection.

We consider that the OFDM receiver gathers  $N$  observation vectors of length  $n_s$ ,  $\mathbf{y}_0, \mathbf{y}_1, \dots, \mathbf{y}_{N-1}$ , to estimate the TO,  $d$ . The initial step for ML derivation is to obtain the joint PDF of the observation vectors under the  $2n_s + 1$  TO hypotheses. We denote this joint PDF given  $H_d$  by  $f_Y(\mathbf{y}|H_d)$ , where

$$\mathbf{y} = [y[0] \ y[1] \ \dots \ y[Nn_s - 1]]^T \quad (15)$$

$$\triangleq [\mathbf{y}_0^T \ \mathbf{y}_1^T \ \dots \ \mathbf{y}_{N-1}^T]^T$$

with

$$y[nn_s + m] \triangleq y_n[m]. \quad (16)$$

as the  $m$ -th sample in the  $n$ -th block. By using the chain rule in probability theory [37], we can write

$$f_Y(\mathbf{y}|H_d) \quad (17)$$

$$= \prod_{n=0}^{N-1} \prod_{m=0}^{n_s-1} f\left(y_n[m] \middle| \bigcap_{u=0}^{m-1} y_n[u], \bigcap_{k=0}^{n-1} \mathbf{y}_k, H_d\right).$$

To obtain the joint PDF in (17), we rely on Theorem 1.

**Theorem 1.** *The elements of the observation vector  $\mathbf{y}$  in (15) irrespective to the value of TO are uncorrelated random variables, i.e.,  $\mathbb{E}\{y_n[u]y_n^*[v]\} = 0, u \neq v$ .*

*Proof:* See Appendix I. ■

Fig. 1 illustrates the scatter plot of the in-phase components of  $y_{10}[100]$  (i.e.,  $y_{10I}[100] = \Re\{y_{10}[100]\}$ ) and  $y_{10}[101]$  (i.e.,  $y_{10I}[101] = \Re\{y_{10}[101]\}$ ) given hypothesis  $H_0$ . As seen, there is no correlation between the two successive samples.

According to Theorem 1, the observation samples in (15) are uncorrelated random variables. Also, we can show that the in-phase  $y_{nI}[m]$  and quadrature  $y_{nQ}[m]$  components of the

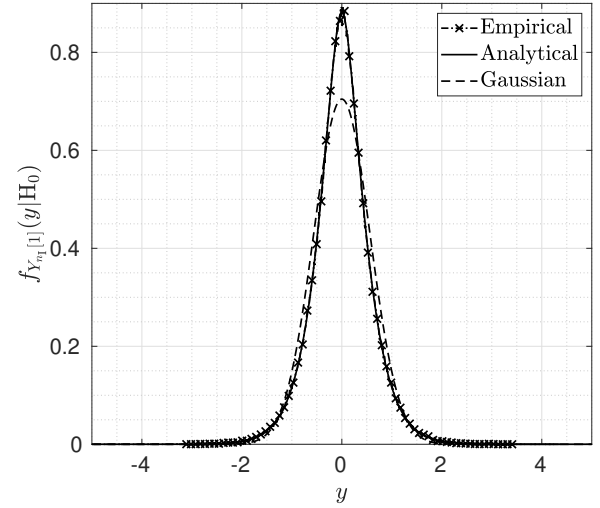


Fig. 2: The empirical and analytical PDFs of  $y_{nI}[1]$  given hypothesis  $H_0$  at 15 dB  $E_b/N_0$  ( $n_x = 128, n_z = 15, n_h = 10, n = 10$ ). The empirical PDF was obtained for  $10^6$  samples.

$m$ -th received sample from the  $n$ -th observation vector, i.e.,  $y_n[m] = y_{nI}[m] + iy_{nQ}[m]$ , are uncorrelated random variables.

Although uncorrelated random variables are not necessarily independent, the independency assumption becomes more valid for the received samples in the case of very fast-varying channels where the maximum Doppler spread of the channel approaches infinity. When the maximum Doppler spread reaches infinity, the channel taps contributing to one received sample become independent from other samples. Moreover, most practical algorithms are particularly sensitive to the distribution and less to correlation. Thus, we can consider that the observation samples are independent random variables to simplify the signal model [38]. Accordingly, we approximate the joint PDF in (17) by the multiplication of the first-order PDFs as

$$f_Y(\mathbf{y}|H_d) \approx \prod_{n=0}^{N-1} \prod_{m=0}^{n_s-1} f_{Y_{nI}[m]}(y_{nI}[m]|H_d) \quad (18)$$

$$\approx \prod_{n=0}^{N-1} \prod_{m=0}^{n_s-1} f_{Y_{nI}[m]}(y_{nI}[m]|H_d) f_{Y_{nQ}[m]}(y_{nQ}[m]|H_d),$$

where  $f_{Y_{nI}[m]}(\cdot|H_d)$  and  $f_{Y_{nQ}[m]}(\cdot|H_d)$  are the PDF of the in-phase and quadrature components of the  $m$ -th received sample from the  $n$ -th observation vector. The accuracy of this assumption is verified in the simulation results.

#### A. PDF Derivation for Delay Hypothesis $H_0$

Theorem (2) provides closed-form expressions for the PDF of the in-phase and quadrature components of the  $m$ -th received sample from the  $n$ -th observation vector given the hypothesis  $H_0$  ( $d = 0$ ). We later show that the conditional PDFs given hypothesis  $H_d$ ,  $d \neq 0$ , can be easily extracted from these PDFs due to the periodicity incurred by the zero-padded guard interval.

**Theorem 2.** *The PDF of the in-phase (quadrature) component of the received samples  $y_{n_I}[m]$  ( $y_{n_Q}[m]$ ),  $m \in \{m \mid 0 \leq m \leq n_s - 1 \text{ when } n < 0\} \cup \{m \mid n_x + n_h - 1 \leq m \leq n_s - 1 \text{ when } n \geq 0\}$  for  $d = 0$  is given by*<sup>1</sup>

$$f_{Y_{n_I}[m]}(y|H_0) = \frac{1}{\sqrt{\pi\sigma_w^2}} \exp\left(-\frac{y^2}{\sigma_w^2}\right). \quad (19)$$

Also, for  $d = 0$  and  $m \in \{m \mid 0 \leq m \leq n_x + n_h - 2 \text{ when } n \geq 0\}$ , we have

$$\begin{aligned} f_{Y_{n_I}[m]}(y|H_0) &= f_{Y_{n_I}[m]}(-y|H_0) \\ &= \left(\prod_{i=a}^b \lambda_i\right)^2 \sum_{j=a}^b \sum_{n=a}^b \frac{e^{\left(\frac{\lambda_j \sigma_w}{2}\right)^2}}{\prod_{k=a, k \neq j}^b (\lambda_k - \lambda_j)} \\ &\quad \times \frac{1}{\prod_{u=a, u \neq j}^b (\lambda_u - \lambda_n)} \frac{1}{(\lambda_j + \lambda_n)} \\ &\quad \times 1/2 \left[ e^{-\lambda_j y} \left( 1 - \Phi\left(\frac{\lambda_j \sigma_w}{2} - \frac{y}{\sigma_w}\right) \right) + \right. \\ &\quad \left. e^{\lambda_j y} \left( 1 - \Phi\left(\frac{\lambda_j \sigma_w}{2} + \frac{y}{\sigma_w}\right) \right) \right], \end{aligned} \quad (20)$$

where  $\lambda_k \triangleq 2/(\sigma_{h_k} \sigma_x)$ ,  $\Phi(x) = \text{erf}(x) = \frac{2}{\sqrt{\pi}} \int_0^x e^{-t^2} dt$  denotes the Gaussian error function, and  $a$  and  $b$  depend on  $m$ , and are given as follows

$$(a, b) = \begin{cases} (0, m) & 0 \leq m \leq n_h - 2 \\ (0, n_h - 1) & n_h - 1 \leq m \leq n_x - 1 \\ (m - n_x + 1, n_h - 1) & n_x \leq m \leq n_x + n_h - 2. \end{cases} \quad (22)$$

Similar expressions hold for  $f_{Y_{n_Q}[m]}(y|H_0)$ .

*Proof:* See Appendix II. ■

Fig. 2 illustrates the derived PDF in (20) for  $y_{n_I}[1]$  given hypothesis  $H_0$  at 15 dB  $E_b/N_0$ . For comparison, we also show the empirical PDF obtained by histogram density estimator and theoretical Gaussian PDF. As seen, the derived PDF accurately matches the empirical PDF. However, it exhibits a larger tail compared to the Gaussian distribution. In Table I, we compare the variance, kurtosis, and skewness of the derived PDF in (20), the empirical histogram density estimation of the PDF, and the Gaussian distribution. The kurtosis measures the fourth-order central moment of the random variable  $Y_{n_I}[1]$  with mean  $\mu \triangleq \mathbb{E}\{Y_{n_I}[1]|H_0\}$ , and the skewness is a measure of the symmetry in the distribution. Large deviation from the mean yields large values of kurtosis. For fair comparison, we consider the normalized kurtosis  $\kappa$  and skewness  $\xi$  defined as

$$\kappa \triangleq \frac{\mathbb{E}\{(Y_{n_I}[1] - \mu)^4\}}{\mathbb{E}^2\{(Y_{n_I}[1] - \mu)^2\}}, \quad (23)$$

and

$$\xi \triangleq \frac{\mathbb{E}\{(Y_{n_I}[1] - \mu)^3\}}{\mathbb{E}^{\frac{3}{2}}\{(Y_{n_I}[1] - \mu)^2\}}. \quad (24)$$

To estimate the normalized kurtosis and skewness for the empirical PDF, we use

$$\hat{\kappa} \triangleq \frac{\frac{1}{M} \sum_{n=0}^{M-1} (y_{n_I}[1] - \hat{\mu})^4}{\left(\frac{1}{M} \sum_{n=0}^{M-1} (y_{n_I}[1] - \hat{\mu})^2\right)^2}, \quad (25)$$

and

$$\hat{\xi} \triangleq \frac{\frac{1}{M} \sum_{n=0}^{M-1} (y_{n_I}[1] - \hat{\mu})^3}{\left(\frac{1}{M} \sum_{n=0}^{M-1} (y_{n_I}[1] - \hat{\mu})^2\right)^{\frac{3}{2}}}, \quad (26)$$

where

$$\hat{\mu} = \frac{1}{M} \sum_{n=0}^{M-1} y_{n_I}[1]. \quad (27)$$

To estimate the kurtosis and skewness in (25) and (26), we set  $M = 10^6$ . As seen in Table I, the theoretical kurtosis obtained by (23) equals the empirical kurtosis in (25) with precision of 0.01. Further, these values are larger than 3; hence, it indicates a non-Gaussian PDF, which in particular, has a larger tail. In Table I, we also observe that for the theoretical and empirical PDFs, the skewness is zero, which implies that the PDF is symmetric around its mean.

### B. PDF Derivation for Delay Hypothesis $H_d$ , $d \neq 0$

In order to obtain the ML estimator, we need to derive the joint PDF of the received samples given all delay hypotheses  $H_d$ ,  $d \in \{-n_s + 1, \dots, -1, 0, 1, \dots, n_s - 1\}$ . In Theorem 2, we derived the PDF of the received samples given hypothesis  $H_0$ , i.e.,  $f_Y(y|H_0)$ . In Appendix III, we prove that  $f_Y(y|H_d)$  can be expressed based on the joint PDF of the received samples given  $H_0$  as it is shown in (28) and (29) at the top of this page, where

$$\begin{aligned} \tilde{f}_{Y[m]}(y|H_0) &\triangleq f_{Y[nn_s+m]}(y|H_0) = f_{Y_n[m]}(y|H_0) \\ &\approx f_{Y_{n_I}[m]}(y_I|H_0) f_{Y_{n_Q}[m]}(y_Q|H_0) \\ &\triangleq f_{Y_I[m]}(y_I|H_0) f_{Y_Q[m]}(y_Q|H_0), \quad n \geq 0 \end{aligned} \quad (30)$$

for  $0 \leq m \leq n_s - 1$ , and

$$\begin{aligned} \tilde{f}_{Y[-]}(y|H_0) &\triangleq f_{Y[nn_s+m]}(y|H_0) = f_{Y_n[m]}(y|H_0), \\ &\approx f_{Y_{n_I}[m]}(y_I|H_0) f_{Y_{n_Q}[m]}(y_Q|H_0) \\ &\triangleq f_{Y_I[-]}(y_I|H_0) f_{Y_Q[-]}(y_Q|H_0), \quad n < 0, \end{aligned} \quad (31)$$

where  $y \triangleq y_I + iy_Q$ ,  $f_{Y[nn_s+m]}(\cdot|H_0)$  is the PDF of the received sample  $y[nn_s + m] \triangleq y_n[m]$  given  $H_0$ , and the PDF of  $\Re\{y[nn_s + m]\} = y_{n_I}[m]$ , i.e.,  $f_{Y_{n_I}[m]}(\cdot|H_0)$  and the PDF of  $\Im\{y[nn_s + m]\} = y_{n_Q}[m]$ , i.e.,  $f_{Y_{n_Q}[m]}(\cdot|H_0)$  are given in Theorem 2. The relation between the PDF of the received samples given  $H_d$  and  $H_0$  is attributed to the periodicity of the zero-padded guard interval.

<sup>1</sup>In Theorem 2, by  $n < 0$ , we mean as if the receiver starts to receive samples before any data is transmitted from the transmitter.

$$\mathbf{f}_{\mathbf{Y}}(\mathbf{y}|\mathbf{H}_d) = \prod_{k=0}^{n_s-d-1} \tilde{f}_{Y[k+d]}(y[k]|\mathbf{H}_0) \prod_{m=1}^{N-1} \left( \prod_{u=0}^{n_s-1} \tilde{f}_{Y[u]}(y[mn_s + u - d]|\mathbf{H}_0) \right) \prod_{v=Nn_s-d}^{Nn_s-1} \tilde{f}_{Y[v-Nn_s+d]}(y[v]|\mathbf{H}_0), \quad d \geq 0 \quad (28)$$

$$\mathbf{f}_{\mathbf{Y}}(\mathbf{y}|\mathbf{H}_d) = \prod_{k=0}^{|d|-1} \tilde{f}_{Y[-]}(y[k]|\mathbf{H}_0) \prod_{m=0}^{N-2} \left( \prod_{u=0}^{n_s-1} \tilde{f}_{Y[u]}(y[mn_s + u - d]|\mathbf{H}_0) \right) \prod_{u=(N-1)n_s-d}^{Nn_s-1} \tilde{f}_{Y[u-(N-1)n_s+d]}(y[u]|\mathbf{H}_0), \quad d < 0 \quad (29)$$

To visualize (28) and (29) of the revised manuscript, let us consider the vector of PDF in (60) in the revised manuscript. We consider the first shown dashed line from the top in the PDF vector as reference line. The elements below this reference line in PDF vector are periodic with period  $n_s$  (see the pattern in Fig. 11 in the revised manuscript). The elements above this reference line represent the PDF of the noise samples. For  $d \geq 0$ , the elements of the observation vector  $\mathbf{y}$  are respectively substituted in the PDF vector starting from the  $(d+1)$ -th element below the reference line. This results in (28). Similarly, for  $d < 0$ , the elements of the observation vector  $\mathbf{y}$  are respectively substituted in the PDF vector starting  $|d|$  elements above the reference line. This results in (29).

### C. ML TO Estimator

The ML estimation for TO is defined to be the value of  $d$  that maximizes  $f_{\mathbf{Y}}(\mathbf{y}|\mathbf{H}_d)$  for  $\mathbf{y}$  fixed, i.e., the value that maximizes the likelihood function. The maximization is performed over the allowable range of  $d$ . Corollary 1 summarizes the proposed NDA-ML TO estimation for ZP-OFDM.

**Corollary 1.** *For a ZP-OFDM system in a doubly-selective fading channel with the received vector  $\mathbf{y}$  in (15), the NDA-ML TO estimator is given by*

$$\hat{d}^{opt} = \underset{d \in \{-n_s+1, \dots, n_s-1\}}{\operatorname{argmax}} \quad \mathbf{f}_{\mathbf{Y}}(\mathbf{y}|\mathbf{H}_d), \quad (32)$$

where  $\mathbf{f}_{\mathbf{Y}}(\mathbf{y}|\mathbf{H}_d)$  is given in (28) and (29).

The proposed time synchronization method can be extended to ZP-OFDM with non-rectangular pulse shaping, but it requires the modification of the PDF in equation (20). In this case, the  $T_{sa}$ -spaced baseband OFDM samples are modeled as independent random variables with different variances, which makes the derivation of the PDF challenging.

Since a closed-form expression cannot be found for the ML estimator in (32), a numerical approach can be used. Numerical methods employ either an exhaustive search or an iterative maximization of the likelihood function.

## IV. LOW-COMPLEXITY IMPLEMENTATION

The derived PDF in (20) is complex due to the integral terms including the Gaussian error function  $\Phi(\cdot)$ . Hence, practical implementation of the proposed ML can be challenging. An alternative approach with feasible implementation and lower complexity is to employ MCS techniques to approximate the

TABLE I: Statistical Analysis

Metric	Empirical	Analytical	Gaussian
Mean	$4.6250 \times 10^{-4}$	0	0
Variance	0.3206	0.3205	0.3206
Skewness	0.0031	0	0
Kurtosis	4.5315	4.5653	3

joint PDF of the received samples. MCS methods benefit from the availability of computer generated random variables to approximate univariate and multidimensional integrals in Bayesian estimation, inference, and optimization problems. The key idea behind MCS method is to generate independent random samples from a PDF usually known up to a normalizing constant. In the following discussion, we use MCS integration method in order to make efficient implementation of the proposed theoretical NDA-ML estimator in (32) possible.

### A. MCS Method

In Appendix II, we proved that  $f_{Y_I[m]}(y_I|\mathbf{H}_0)$  in (20) is expressed in an integral form as follows

$$\begin{aligned} f_{Y_{n_I}[m]}(y_I|\mathbf{H}_0) &= \int_{-\infty}^{\infty} f_{W_{n_I}[m]}(y_I - v) f_{V_{n_I}[m]}(v|\mathbf{H}_0) dv \\ &= \int_{-\infty}^{\infty} \frac{1}{\sqrt{\pi\sigma_w^2}} \exp \left\{ -\frac{1}{\sigma_w^2} (y_I - v)^2 \right\} f_{V_{n_I}[m]}(v) dv, \end{aligned} \quad (33)$$

where

$$\begin{aligned} f_{V_{n_I}[m]}(v|\mathbf{H}_0) &= \left( \prod_{i=a}^b \lambda_i \right)^2 \sum_{j=a}^b \sum_{n=a}^b \frac{1}{\prod_{k=a, k \neq j}^b (\lambda_k - \lambda_j)} \\ &\quad \times \frac{1}{\prod_{p=a, p \neq j}^b (\lambda_p - \lambda_n)} \frac{e^{-\lambda_j |v|}}{\lambda_j + \lambda_n}, \end{aligned} \quad (34)$$

and  $f_{W_{n_I}[m]}(w)$  is the PDF of the white Gaussian noise with variance  $\sigma_w^2/2$ . Generating samples from random variable  $V_{n_I}[m]$  with PDF in (34) is straightforward since it is expressed as a linear function of independent exponentially distributed random variables with rate parameter  $\lambda_k = (\sigma_{h_k} \sigma_x/2)^{-1}$  as shown in (49) of Appendix II.

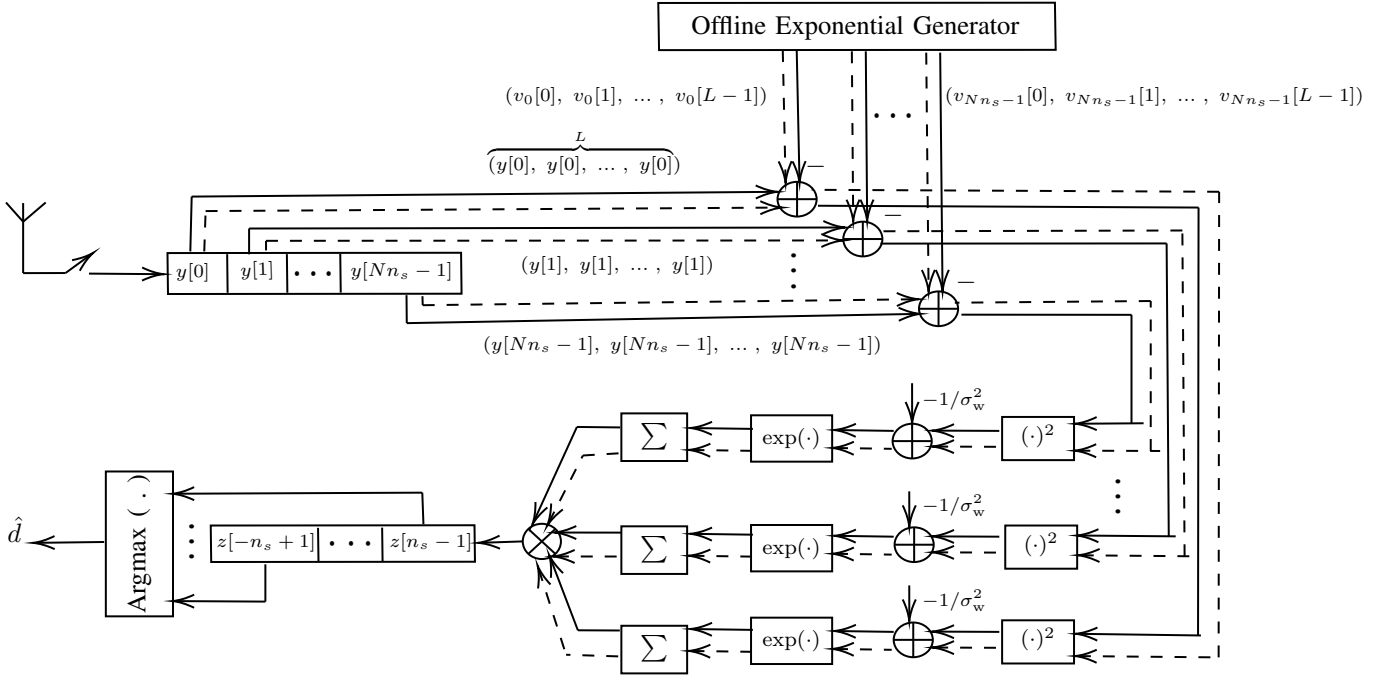


Fig. 3: MCS implementation of the proposed theoretical NDA-ML TO estimator in (32) using (36). The solid and dashed lines represent the in-phase and quadrature components of the received samples, respectively.

By using Monte Carlo integration method, we can write

$$f_{Y_{n_I}[m]}(y_I|H_0) \simeq \frac{1}{L} \sum_{\ell=0}^{L-1} \frac{1}{\sqrt{\pi\sigma_w^2}} \exp \left\{ -\frac{1}{\sigma_w^2} (y_I - v_\ell)^2 \right\}, \quad (35)$$

where  $L$  is the number of Monte Carlo samples, and  $\{v_0, v_1, \dots, v_{L-1}\}$  are i.i.d samples drawn from  $V_{n_I}[m]$ . By applying Monte Carlo integration to the marginal PDFs of the in-phase and quadrature components of  $\mathbf{y}$ , the joint PDF is given by

$$\begin{aligned} f_{\mathbf{Y}}(\mathbf{y}|H_0) &\approx \prod_{n=0}^{N-1} \prod_{m=0}^{n_s-1} f_{Y_{n_I}[m]}(y_{n_I}[m]|H_0) f_{Y_{n_Q}[m]}(y_{n_Q}[m]|H_0) \\ &\simeq \frac{1}{(\pi\sigma_w^2)^{Nn_s}} \prod_{n=0}^{N-1} \prod_{m=0}^{n_s-1} \left( \sum_{\ell=1}^L \exp \left\{ \frac{-1}{\sigma_w^2} (y_{n_I}[m] - v_{n_I}^m[\ell])^2 \right\} \right) \\ &\quad \times \sum_{\ell=1}^L \exp \left\{ \frac{-1}{\sigma_w^2} (y_{n_Q}[m] - v_{n_Q}^m[\ell])^2 \right\}, \end{aligned} \quad (36)$$

where  $v_{n_I}^m[\ell]$  and  $v_{n_Q}^m[\ell]$  are i.i.d values drawn from random variables with PDFs  $f_{V_{n_I}[m]}(v)$  and  $f_{V_{n_Q}[m]}(v)$ , respectively. By using (36), we can design the MCS implementation of the theoretical NDA-ML TO estimator in (32) as in Fig. 3.

### B. Iterative Likelihood Maximization

Efficient one dimensional iterative search algorithms can be used to avoid exhaustive search, and thus, reduce the

computational complexity of (32). In iterative search method, an interval  $[d_L, d_U]$  containing the true TO  $d^*$  is established and is then repeatedly reduced on the basis of function evaluations until a reduced bracket  $[d_L, d_U]$  is achieved which is sufficiently small. The minimizer/maximizer can be assumed to be at the center of interval  $[d_L, d_U]$ . These methods can be applied to any function and differentiability of the function is not essential.

An iterative search method in which iterations can be performed until the desired accuracy in either the maximizer or the maximum value of the objective function is achieved is the golden-section search method [39]. For a strictly unimodal function with an extremum inside the interval, Golden-section search method finds that extremum, while for an interval containing multiple extrema (possibly including the interval boundaries), it converges to one of them. Implementation of the proposed NDA-ML TO estimation with golden-section search is summarized in Algorithm 1. For Algorithm 1, we define

$$\mathcal{L}(d) \triangleq \text{Prod} \left( f_{\mathbf{Y}}^{(d:d+Nn_s-1)}(\mathbf{y}; H_0) \right), \quad (37)$$

where  $\text{Prod}([z_0, z_1, \dots, z_{u-1}]) \triangleq \prod_{i=0}^{u-1} z_i$ , and

$$\begin{aligned} \mathbf{f}_{\mathbf{Y}}^{(d:q)}(\cdot; H_0) &\triangleq \\ &\left[ f_{Y[d]}(\cdot|H_0) f_{Y[d+1]}(\cdot|H_0) \dots f_{Y[q]}(\cdot|H_0) \right]^T \end{aligned} \quad (38)$$

with  $q \geq d$  and  $f_{Y[nn_s+d]}(\cdot|H_0)$  as the PDF of the received sample  $y[nn_s + d] \triangleq y_n[d]$  given  $H_0$ .

**Algorithm 1** Golden-section search

---

**Initialization:**  $\mathcal{D} \leftarrow \{-n_s, \dots, n_s - 2\}$ ,  $init \leftarrow -n_s + 1$ ,  
 $last \leftarrow n_s - 1$ ,  $ratio \leftarrow 0.381966$

```

1:  $c \leftarrow init + \lfloor ratio * (last - init) \rfloor$ 
2: while  $\mathcal{L}(c) < \mathcal{L}(init)$  or  $\mathcal{L}(c) < \mathcal{L}(last)$  do
3:   if  $|\mathcal{D}|=2$  then
4:     if  $\mathcal{L}(init) > \mathcal{L}(last)$  then
5:       return  $\hat{d}^{opt} \leftarrow init$ 
6:     else
7:       return  $\hat{d}^{opt} \leftarrow last$ 
8:    $\mathcal{D} \leftarrow \mathcal{D} \setminus \{c\}$ 
9:    $c \leftarrow$  Choose a random index from the set  $\mathcal{D}$ 
10: while  $last - init \geq 4$  do
11:   if  $last - c \geq c - init$  then
12:      $d \leftarrow c + \lfloor ratio * (last - init) \rfloor$ 
13:     if  $\mathcal{L}(d) < \mathcal{L}(c)$  then
14:        $last \leftarrow d$ 
15:   else
16:      $init \leftarrow c$ 
17:      $c \leftarrow d$ 
18:   else
19:      $d \leftarrow c - \lfloor ratio * (last - init) \rfloor$ 
20:     if  $\mathcal{L}(d) < \mathcal{L}(c)$  then
21:        $init \leftarrow d$ 
22:   else
23:      $last \leftarrow c$ 
24:      $c \leftarrow d$ 
25:  $\hat{d}^{opt} \leftarrow \operatorname{argmax}_{i \in \{init, \dots, last\}} \mathcal{L}(i)$ 
26: return  $\hat{d}^{opt}$ 

```

---

**C. Complexity Analysis**

Here, we compare the complexity of the proposed theoretical and the MCS time synchronization algorithms. In our complexity analysis, a real addition, multiplication, or division is counted as one floating point operation (FLOP). Considering the fact that the number of FLOPs for  $H_d$ ,  $d \geq 0$ , is higher than that for  $d < 0$ , the number of FLOPs per TO hypothesis for the theoretical and the MCS time synchronization algorithms are upper bounded by  $2N(n_x + n_z) + (2N - 1)n_x n_h (8 + 2u_1 + 2u_2)$  and  $((6 + 2u_1)(L - 1) + 1)(n_x + n_z - 1)(N - 1)$ , respectively, where  $u_1$  and  $u_2$  denote the number of FLOPs for the computation of  $\exp(\cdot)$  and error function  $\Phi(\cdot)$ , respectively. Here,  $L$  is a trade-off parameter between the accuracy and complexity for the MCS algorithm. That is, increasing  $L$  increases both accuracy and complexity of the MCS algorithm.

The ratio of the average estimation time (RAET) versus  $n_x$  for the proposed theoretical NDA-ML and the MCS algorithms are shown in Table II. Here, RAET is defined as:

$$\text{RAET} = \frac{\text{Average estimation time for MCS}}{\text{Average estimation time for the theoretical}}. \quad (39)$$

The number of Monte Carlo samples is set to  $L = 10^4$  for the MCS implementation, and exhaustive search method is used for both algorithms. As seen, MCS implementation offers a lower computational complexity compared to the theoretical ML estimator using Theorem 2. This complexity reduction

TABLE II: Complexity Analysis

$n_x$	64	128	256	512	1024
RAET	0.841	0.779	0.704	0.668	0.629

is obtained at the expense of an insignificant performance degradation in terms of lock-in probability as it will be shown in the next section.

**V. SIMULATIONS**

In this section, we evaluate the performance of the proposed NDA-ML time synchronization algorithm through several simulation experiments.

**A. Simulation Setup**

We consider a ZP-OFDM system with 128-QAM modulation in a frequency-selective Rayleigh fading channel. Unless otherwise mentioned, the number of sub-carriers is  $n_x = 128$ , the number of zero-padded samples is  $n_z = 15$ , and the number of observed OFDM symbols at the receiver is  $N = 10$ . The sampling time of the ZP-OFDM system at the receiver is  $T_{sa} = 10^{-6}$ s. An uncorrelated multipath fading channel with  $n_h = 10$  taps and maximum delay spread of  $\tau_{max} = 10\mu\text{s}$  is considered. The delay profile of the Rayleigh fading channel in (6) is modeled as an exponential-decay function, i.e.,  $\sigma_{h_l}^2 = \alpha \exp(-\beta l)$ ,  $l = 0, 1, \dots, n_h - 1$ , where  $p_h = \sum_{l=0}^{n_h-1} \sigma_{h_l}^2 = 1$ ,  $\alpha = 1/2.5244$ , and  $\beta = 0.5$ . The maximum Doppler spread of the fading channel is set to  $f_D = 5$  Hz. Without loss of generality, the transmit power is assumed to be  $\sigma_x^2 = 1$ , and the AWGN is modeled as a zero-mean complex Gaussian random variable with variance  $\sigma_w^2$ , which varies according to the value of SNR  $\gamma \triangleq \sigma_x^2 p_h / \sigma_w^2$ . The TO introduced to the system is modeled as a uniformly distributed integer random variable in the range of  $d \in [-30, 30]$ . Simulations are evaluated under  $10^4$  Monte Carlo realizations, and the number of samples for MCS implementation of the proposed theoretical NDA-ML algorithm is  $L = 10^4$ . The performance of the proposed algorithms are evaluated in terms of mean squared error (MSE) and lock-in probability. Here, the lock-in probability is defined as the probability that the estimated TO (given in sampling time) equals to the actual TO. That is, any non-zero error is counted as a missed estimation.

**B. Simulation Results**

The performance of the proposed theoretical NDA-ML algorithm, its MCS implementation, and the current state-of-the-art NDA TO estimator for ZP-OFDM, i.e. transition metric (TM) [28], for different values of  $E_b/N_0$  are shown in Fig. 4. As can be seen, the proposed theoretical algorithm and its MCS implementation outperform the TM algorithm since they maximize the likelihood function while TM is a heuristic algorithm. Moreover, as seen, there is a negligible performance gap between the proposed theoretical NDA-ML algorithm and its MCS implementation. This performance gap

can be further reduced by increasing the number of Monte Carlo samples  $L$  used for averaging in (36) at the expense of higher complexity. In Fig. 4, we also illustrate the performance of the sub-optimal time synchronization algorithm in [40], which relies on Gaussian PDF approximation of the received samples. As can be seen, there is a large gap between the proposed algorithms and the sub-optimal algorithm in [40] at low SNR values.

Fig. 5 illustrates the effect of the maximum Doppler spread (mobility) on the performance of the proposed theoretical NDA-ML algorithm and its MCS implementation. As seen, the lock-in probability increases as the maximum Doppler spread increases. The reason is that the time dynamics of the channel taps contributing (through convolution) to the received samples become less correlated as the maximum Doppler spread increases. However, for zero maximum Doppler spread, identical channel taps contribute to the received samples. Thus, our independency assumption on the received samples becomes more valid for higher values of maximum Doppler spread. These results reveal that the proposed NDA-ML algorithm can be considered as a promising candidate for vehicle-to-vehicle (V2V) communications.

The effect of the number of OFDM symbols  $N$ , used for time synchronization, on the performance of the proposed theoretical NDA-ML algorithm, its MCS implementation, and the TM algorithm [28] are represented in Fig. 6. As expected, the higher  $N$ , the higher the lock-in probability. Major improvements in performance occurs when the number of OFDM symbols increases from 1 to 10, and then the rate of performance improvement decreases. This is due to the fact that innovation introduced by each new sample to an ML estimator decreases as the total number of samples (used for estimation) increases.

In Fig. 7, the performance of the proposed theoretical NDA-ML TO estimator, its MCS implementation, and the TM estimator [28] versus the number of channel taps  $n_h$  for  $n_z = 20$  at 15 dB  $E_b/N_0$  are shown. As seen, the lock-in probability of the theoretical NDA-ML TO estimator and its MCS implementation degrades as  $n_h$  increases. This is because the sharpness of the likelihood function decreases; the sharpness of likelihood function determines how accurately we can estimate an unknown parameter.

In Fig. 8, we illustrate the empirical probability mass function (PMF) of the synchronization error for the proposed theoretical and the MCS algorithms at 10 dB  $E_b/N_0$ . As can be seen, the empirical PMF of the error is not symmetric around zero and is slightly biased towards positive TOs. Based on asymptotic properties of the MLEs, the biased term approaches zero as  $N \rightarrow \infty$ . Moreover, we observe that the synchronization error falls in small interval, i.e.,  $\{-2, -1, 1, 2\}$ . This means that the proposed algorithms offer low MSE as shown in Fig. 9. Because of low MSE, the proposed time-synchronization algorithms can take advantage of low complexity channel coding to further improve synchronization performance.

The effect of PDP estimation error on the performance of the proposed theoretical and the MCS time synchronization algorithms is shown in Fig. 10. We model the estimated PDP

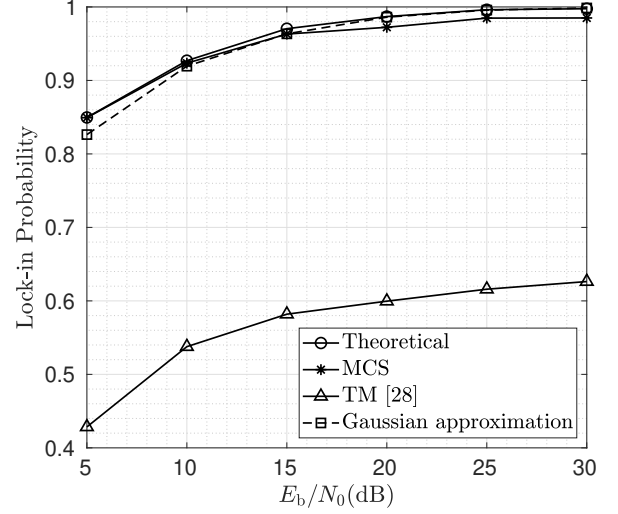


Fig. 4: Lock-in probability versus  $E_b/N_0$ .

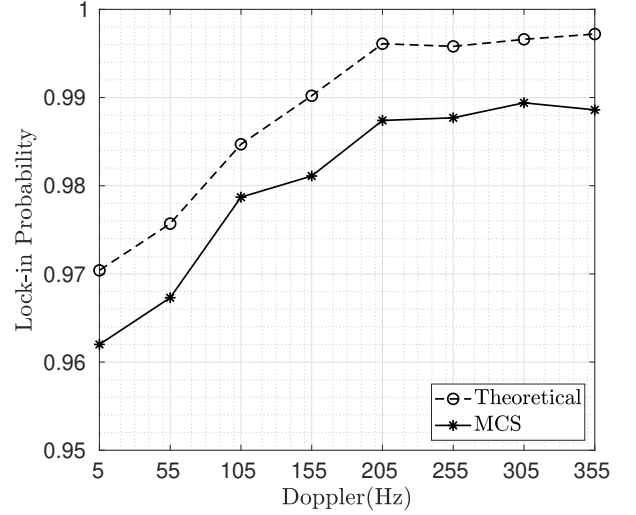


Fig. 5: Lock-in probability versus maximum Doppler spread of the fading channel at 15 dB  $E_b/N_0$ .

as

$$\hat{\sigma}_{h_k}^2 \in \mathcal{U}[\sigma_{h_k}^2 - \alpha\sigma_{h_k}^2, \sigma_{h_k}^2 + \alpha\sigma_{h_k}^2], \quad (40)$$

where  $\sigma_{h_k}^2$ ,  $k = 0, 1, \dots, n_h - 1$ , is the true PDP, and  $\mathcal{U}[a, b]$  denotes the uniform distribution in the interval  $[a, b]$ . In Fig. 10, we show the lock-in probability versus  $\alpha \in [0, 1]$  at 10 dB  $E_b/N_0$ . As can be seen, the theoretical and the MCS algorithms are robust to the delay profile estimation error for  $\alpha \in [0, 1]$  and  $\alpha \in [0, 0.5]$ , respectively. While the performance of the theoretical algorithm slightly degrades for  $\alpha \in [0.5, 1]$ , the lock-in probability is still larger than 0.75.

## VI. CONCLUSIONS

In this paper, for the first time in the literature, the NDA-ML time synchronization for ZP-OFDM was analytically derived

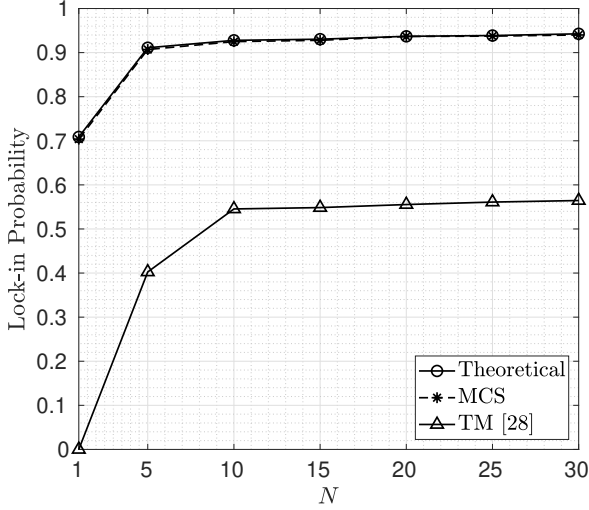


Fig. 6: Lock-in probability versus the number of observation vectors  $N$  at 10 dB  $E_b/N_0$ .

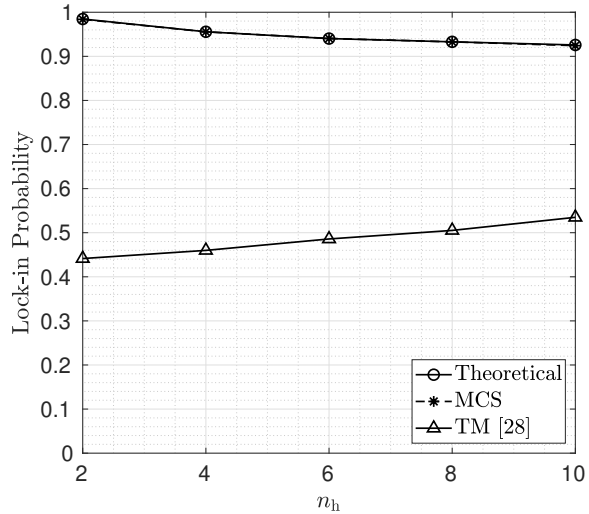


Fig. 7: Lock-in probability versus the number of channel taps  $n_h$  at 10 dB  $E_b/N_0$ .

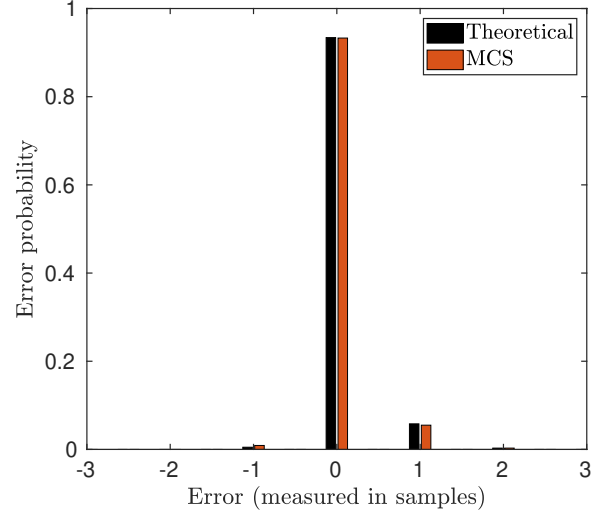


Fig. 8: PMF of the synchronization error for the theoretical and the MCS algorithms at 10 dB  $E_b/N_0$ .

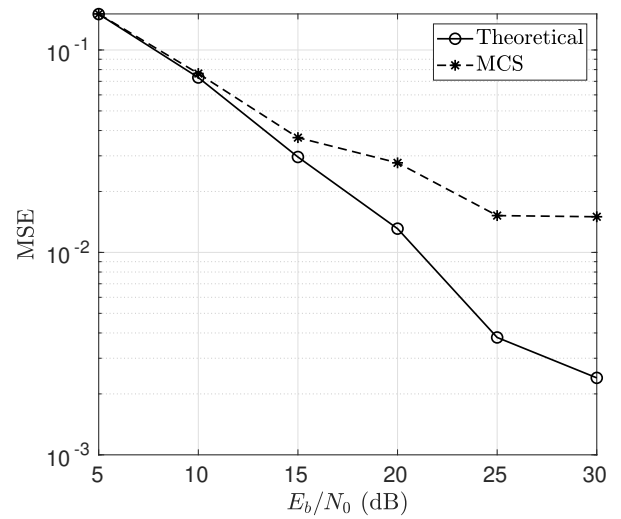


Fig. 9: Mean Squared Error (MSE) versus SNR for Theoretical and MCS method.

and a feasible solution for its implementation based on MCS technique was proposed. The obtained time synchronization method can be employed for both frame and symbol synchronization. Moreover, to achieve the optimal time synchronization method, we obtained a closed-form approximate expression for the distribution of convolution, i.e. received convolved signal. Simulation results verify that the proposed theoretical NDA-ML time synchronization and its MCS implementation can offer high lock-in probabilities even at low SNR values. Also, they are effective in highly time-selective channels with large maximum Doppler spread. These properties make ZP-OFDM a promising candidate for low-power IoT networks and V2V communications.

## REFERENCES

- [1] B. Farhang-Boroujeny and H. Moradi, "OFDM inspired waveforms for 5G," *IEEE Commun. Surveys Tuts.*, vol. 18, no. 4, pp. 2474–2492, 4Q, 2016.
- [2] X. Zhang, L. Zhang, P. Xiao, and J. Wei, "Fine timing synchronization based on modified expectation maximization clustering algorithm for OFDM systems," *IEEE Commun. Lett.*, vol. 8, no. 5, pp. 1452–1455, Oct. 2019.
- [3] H. Abdzadeh-Ziabari, W.-P. Zhu, and M. Swamy, "Timing and frequency synchronization and doubly selective channel estimation for OFDMA uplink," *IEEE Trans. Circuits Syst. II*, vol. 67, no. 1, pp. 62–66, Jan. 2020.
- [4] X. Zhang, J. Liu, H. Li, and B. Himed, "Maximum likelihood syn-

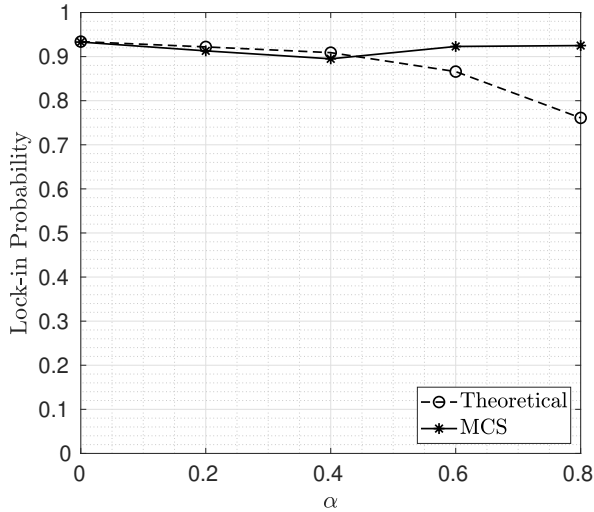


Fig. 10: Sensitivity of the proposed time synchronization algorithms to PDP estimation error for  $N = 10$  at 10 dB  $E_b/N_0$ .

- chronization for DVB-T2 in unknown fading channels," *IEEE Trans. Broadcast.*, vol. 61, no. 4, pp. 615–624, Dec. 2015.
- [5] A. Mohebbi, H. Abdzadeh-Ziabari, and M. G. Shayesteh, "Novel coarse timing synchronization methods in OFDM systems using fourth-order statistics," *IEEE Trans. Veh. Technol.*, vol. 64, no. 5, pp. 1904–1917, May 2014.
  - [6] M. Morelli, C.-C. J. Kuo, and M.-O. Pun, "Synchronization techniques for orthogonal frequency division multiple access (OFDMA): A tutorial review," *Proc. IEEE*, vol. 95, no. 7, pp. 1394–1427, Jul. 2007.
  - [7] B. Park, H. Cheon, E. Ko, C. Kang, and D. Hong, "A blind OFDM synchronization algorithm based on cyclic correlation," *IEEE Signal Process. Lett.*, vol. 11, no. 2, pp. 83–85, Feb. 2004.
  - [8] D. W. Lin, "An analysis of the performance of ML blind OFDM symbol timing estimation," *IEEE Trans. Signal Process.*, vol. 66, no. 20, pp. 5324–5337, Oct. 2018.
  - [9] H. Abdzadeh-Ziabari, W. Zhu, and M. N. S. Swamy, "Joint maximum likelihood timing, frequency offset, and doubly selective channel estimation for OFDM systems," *IEEE Trans. Veh. Technol.*, vol. 67, no. 3, pp. 2787–2791, Mar. 2018.
  - [10] H. Abdzadeh-Ziabari, W.-P. Zhu, and M. Swamy, "Improved coarse timing estimation in OFDM systems using high-order statistics," *IEEE Trans. Commun.*, vol. 64, no. 12, pp. 5239–5253, 2016.
  - [11] M. M. U. Gul, X. Ma, and S. Lee, "Timing and frequency synchronization for OFDM downlink transmissions using Zadoff-Chu sequences," *IEEE Trans. Wireless Commun.*, vol. 14, no. 3, pp. 1716–1729, Mar. 2015.
  - [12] A. A. Nasir, S. Durrani, H. Mehrpouyan, S. D. Blostein, and R. A. Kennedy, "Timing and carrier synchronization in wireless communication systems: a survey and classification of research in the last 5 years," *EURASIP Journal on Wireless Communications and Networking*, vol. 2016, no. 1, p. 180, Aug. 2016.
  - [13] I. B. F. de Almeida, L. L. Mendes, J. J. Rodrigues, and M. A. da Cruz, "5G waveforms for IoT applications," *IEEE Commun. Surveys Tuts.*, vol. 21, no. 3, pp. 2554–2567, 3Q. 2019.
  - [14] S. Venkatesan and R. A. Valenzuela, "OFDM for 5G: Cyclic prefix versus zero postfix, and filtering versus windowing," in *Proc. IEEE ICC*, Kuala Lumpur, Malaysia, May 2016, pp. 1–5.
  - [15] P.-S. Wang and D. W. Lin, "On maximum-likelihood blind synchronization over WSSUS channels for OFDM systems," *IEEE Trans. Signal Process.*, vol. 63, no. 19, pp. 5045–5059, Oct. 2015.
  - [16] W.-L. Chin, "Blind symbol synchronization for OFDM systems using cyclic prefix in time-variant and long-echo fading channels," *IEEE Trans. Veh. Technol.*, vol. 61, no. 1, pp. 185–195, Jan. 2012.
  - [17] J.-J. Van de Beek, M. Sandell, and P. O. Borjesson, "ML estimation of time and frequency offset in OFDM systems," *IEEE Trans. Signal Process.*, vol. 45, no. 7, pp. 1800–1805, Jul. 1997.
  - [18] Z. Wang, S. Zhou, G. B. Giannakis, C. R. Berger, and J. Huang, "Frequency-domain oversampling for zero-padded OFDM in underwater acoustic communications," *IEEE J. Ocean. Eng.*, vol. 37, no. 1, pp. 14–24, Jan. 2012.
  - [19] B. Su and P. Vaidyanathan, "New blind block synchronization for transceivers using redundant precoders," *IEEE Trans. Signal Process.*, vol. 56, no. 12, pp. 5987–6002, Dec. 2008.
  - [20] J. Wang, J. Song, Z.-X. Yang, L. Yang, and J. Wang, "Frames theoretic analysis of zero-padding OFDM over deep fading wireless channels," *IEEE Trans. Broadcast.*, vol. 52, no. 2, pp. 252–260, Jun. 2006.
  - [21] D. Van Welden, H. Steendam, and M. Moeneclaey, "Iterative decision-directed joint frequency offset and channel estimation for KSP-OFDM," *IEEE Trans. Commun.*, vol. 60, no. 10, pp. 3103–3110, Oct. 2012.
  - [22] B. Muquet, Z. Wang, G. B. Giannakis, M. de Courville, and P. Duhamel, "Cyclic prefixing or zero padding for wireless multicarrier transmissions?" *IEEE Trans. Commun.*, vol. 50, no. 12, pp. 2136–2148, Dec. 2002.
  - [23] Y. Li, H. Minn, and R. Rajatheva, "Synchronization, channel estimation, and equalization in MB-OFDM systems," *IEEE Trans. Wireless Commun.*, vol. 7, no. 11, pp. 4341–4352, Nov. 2008.
  - [24] C.-D. Chung and W.-C. Chen, "Preamble sequence design for spectral compactness and initial synchronization in OFDM," *IEEE Trans. Veh. Technol.*, vol. 67, no. 2, pp. 1428–1443, Feb. 2018.
  - [25] J. A. Zhang and X. Huang, "Autocorrelation based coarse timing with differential normalization," *IEEE Trans. Wireless Commun.*, vol. 11, no. 2, pp. 526–530, Feb. 2011.
  - [26] H. Abdzadeh-Ziabari and M. G. Shayesteh, "A novel preamble-based frame timing estimator for OFDM systems," *IEEE Commun. Lett.*, vol. 16, no. 7, pp. 1121–1124, July 2012.
  - [27] B. Sheng, J. Zheng, X. You, and L. Chen, "A novel timing synchronization method for OFDM systems," *IEEE Commun. Lett.*, vol. 14, no. 12, pp. 1110–1112, Dec. 2010.
  - [28] V. Le Nir, T. van Waterschoot, J. Duplity, and M. Moonen, "Blind coarse timing offset estimation for CP-OFDM and ZP-OFDM transmission over frequency selective channels," *EURASIP Journal on Wireless Communications and Networking*, vol. 2009, no. 1, p. 262813, Jan. 2010. [Online]. Available: <https://doi.org/10.1155/2009/262813>
  - [29] H. Bolcskei, "Blind estimation of symbol timing and carrier frequency offset in wireless OFDM systems," *IEEE Trans. Commun.*, vol. 49, no. 6, pp. 988–999, Jun. 2001.
  - [30] Y. G. Li and G. L. Stuber, *Orthogonal frequency division multiplexing for wireless communications*. Springer Science, 2006.
  - [31] T. Hwang, C. Yang, G. Wu, S. Li, and G. Y. Li, "OFDM and its wireless applications: A survey," *IEEE Trans. Veh. Technol.*, vol. 58, no. 4, pp. 1673–1694, May 2009.
  - [32] G. Forney, "Delay profile - an overview," *IEEE Trans. Inf. Theory*, vol. 18, no. 3, pp. 363–378, May 1972.
  - [33] A. L. Swindlehurst, "Time delay and spatial signature estimation using known asynchronous signals," *IEEE Transactions on Signal Processing*, vol. 46, no. 2, pp. 449–462, 1998.
  - [34] R. Roy and T. Kailath, "Esprit-estimation of signal parameters via rotational invariance techniques," *IEEE Transactions on acoustics, speech, and signal processing*, vol. 37, no. 7, pp. 984–995, 1989.
  - [35] Y. Liu, Z. Tan, H. Hu, L. J. Cimini, and G. Y. Li, "Channel estimation for OFDM," *IEEE Communications Surveys & Tutorials*, vol. 16, no. 4, pp. 1891–1908, 2014.

- [36] P. Banelli, "Theoretical analysis and performance of OFDM signals in nonlinear fading channels," *IEEE Trans. Wireless Commun.*, vol. 2, no. 2, pp. 284–293, Mar. 2003.
- [37] A. Leon-Garcia, *Probability and random processes for electrical engineering*. Pearson Education India, 1994.
- [38] S. M. Kay, *Fundamentals of statistical signal processing: Practical algorithm development*. Pearson Education, 2013, vol. 3.
- [39] W. H. Press, S. A. Teukolsky, W. T. Vetterling, and B. P. Flannery, *Numerical recipes 3rd edition: The art of scientific computing*. Cambridge university press, Sep. 2007.
- [40] K. Pourtahmasi Roshandeh, M. Mohammadkarimi, and M. Ardakani, "An Approximate Maximum Likelihood Time Synchronization Algorithm for Zero-padded OFDM in Channels with Impulsive Gaussian Noise," *arXiv e-prints*, p. arXiv:2008.06586, Aug. 2020.
- [41] M. K. Simon, *Probability distributions involving Gaussian random variables: A handbook for engineers and scientists*. Springer Science & Business Media, May 2007.
- [42] M. Bibinger, "Notes on the sum and maximum of independent exponentially distributed random variables with different scale parameters," *arXiv preprint arXiv:1307.3945*, Jul. 2013.
- [43] I. S. Gradshteyn and I. M. Ryzhik, *Table of integrals, series, and products*. Academic press, May 2014.

#### APPENDIX I PROOF OF THEOREM 1

Let us define sequences  $\mathcal{S}$  and  $\mathcal{Y}$  as follows

$$\begin{aligned}\mathcal{S} &\triangleq \{\dots, \tilde{s}[-1], \tilde{s}[0], \tilde{s}[1], \dots\} \\ &= \{\dots, 0, 0, \mathbf{s}_0^T, \mathbf{s}_1^T, \dots\},\end{aligned}\quad (41)$$

and

$$\mathcal{Y} \triangleq \{\dots, \tilde{y}[-1], \tilde{y}[0], \tilde{y}[1], \dots\}, \quad (42)$$

where  $\mathbf{s}_n$  is defined in (11),  $\tilde{s}[nn_s + m] \triangleq \mathbf{s}_n[m]$ , and

$$\tilde{y}[u] = \sum_{l=0}^{n_h-1} h[l] \tilde{s}[u-l] + w[u]. \quad (43)$$

with  $w[u] \sim \mathcal{CN}(0, \sigma_w^2)$  as AWGN

Since  $\mathcal{S}$  is composed of OFDM samples  $x_n(mT_{sa})$ , which are modeled as zero-mean i.i.d complex Gaussian random variables, and zero-padded elements, we have

$$\mathbb{E}\{\tilde{y}[u]\} = 0, \quad (44)$$

and

$$\mathbb{E}\{\tilde{s}[v] \tilde{s}^*[u]\} = 0, \quad v \neq u. \quad (45)$$

For  $u = v$ , we either have  $\mathbb{E}\{\tilde{s}[v] \tilde{s}^*[u]\} = 0$  or  $\mathbb{E}\{\tilde{s}[v] \tilde{s}^*[u]\} = \sigma_x^2$ , where the former is valid for the zero-padded samples, and the latter is obtained from (13) for OFDM samples. Since the noise component  $w[n]$  in (43) is zero-mean AWGN, we can write<sup>2</sup>

$$\mathbb{E}\{\tilde{y}[u] \tilde{y}^*[v]\} = \sigma_x^2 \sum_{l=0}^{n_h-1} \mathbb{E}\{h[l] h^*[v-u+l]\}, \quad (46)$$

<sup>2</sup>It is obvious that for the observation samples containing noise only samples,  $\mathbb{E}\{\tilde{y}[u] \tilde{y}^*[v]\} = 0, v \neq u$ .

where  $u \neq v$ . Because the channel taps in (6) are uncorrelated random variables, we can write

$$\mathbb{E}\{\tilde{y}[u] \tilde{y}^*[v]\} = 0, \quad u \neq v, \quad (47)$$

which implies that  $\tilde{y}[u]$  and  $\tilde{y}[v]$  are also uncorrelated random variables.

Finally, we can easily conclude that the elements of  $\mathbf{y}$  given hypothesis  $H_d$  share the same property with  $\mathcal{Y}$  in the context of correlation since  $\mathbf{y}$  is obtained by windowing  $\mathcal{Y}$ .

#### APPENDIX II PROOF OF THEOREM 2

Let us write the in-phase component of the received sample in (4) as follows

$$y_{n_1}[m] = v_{n_1}[m] + w_{n_1}[m], \quad (48)$$

where  $y_{n_1}[m] \triangleq \Re\{y_n[m]\}$ ,  $w_{n_1}[m] \triangleq \Re\{w_n[m]\}$ , and

$$v_{n_1}[m] \triangleq \Re\{v_n[m]\} = \Re\left\{\sum_{l=0}^{n_h-1} h[l] s_n[m-l]\right\}.$$

We consider that  $v_{n_1}[m]$  and  $w_{n_1}[m]$  are the realizations of the random variables  $V_{n_1}[m]$  and  $W_{n_1}[m]$ , respectively. We also denote the PDF of  $V_{n_1}[m]$  and  $W_{n_1}[m]$  with  $f_{V_{n_1}[m]}(v|H_0)$  and  $f_{W_{n_1}[m]}(w|H_0)$ .

Case 1:  $m \in \{m \mid 0 \leq m \leq n_s - 1 \text{ when } n < 0\} \cup \{m \mid n_x + n_h - 1 \leq m \leq n_s - 1 \text{ when } n \geq 0\}$

Let us write  $v_{n_1}[m]$  as equation (44), at the top of the next page, where  $h_I[l] \triangleq \Re\{h[l]\}$ ,  $h_Q[l] \triangleq \Im\{h[l]\}$ ,  $x_{n_1}[m] \triangleq \Re\{x_n[m]\}$ , and  $x_{n_Q}[m] \triangleq \Im\{x_n[m]\}$ . By replacing (44) into (48), we can write (see Fig. 11)

$$y_{n_1}[m] = w_{n_1}[m], \quad n_x + n_h - 1 \leq m \leq n_s - 1. \quad (45)$$

Also, given  $H_0$ , we have

$$y_{n_1}[m] = w_{n_1}[m], \quad n < 0. \quad (46)$$

By using  $W_{n_1}[m] \sim f_{W_{n_1}[m]}(w|H_0) = \mathcal{CN}(0, \sigma_w^2/2)$ , (45), and (46), we obtain (19).

Case 2:  $m \in \{m \mid 0 \leq m \leq n_x + n_h - 2 \text{ when } n \geq 0\}$

Since  $W_{n_1}[m]$  and  $V_{n_1}[m]$  are independent random variables, we can write the PDF of  $y_{n_1}[m]$  in (48) given hypothesis  $H_0$  as the convolution of their PDFs. Prior to convolution derivation, we first need to derive the PDF of  $V_{n_1}[m]$  for  $0 \leq m \leq n_x + n_h - 2$ . To obtain the PDF of  $V_{n_1}[m]$ , we can employ the characteristic function (CHF) method.

By using (6.1) in [41] and (44), we can write the CHF of  $V_{n_1}[m]$  given  $H_0$  as follows

$$\begin{aligned}\phi_{V_{n_1}[m]|H_0}(t) &\triangleq \frac{1}{\prod_{k=a}^b} \left(1 + \frac{\sigma_{h_k}^2 \sigma_x^2 t^2}{4}\right) \\ &= \prod_{k=a}^b \frac{1}{\left(1 + j \frac{\sigma_{h_k} \sigma_x}{2} t\right)} \frac{1}{\left(1 - j \frac{\sigma_{h_k} \sigma_x}{2} t\right)}\end{aligned}\quad (47)$$

for  $0 \leq m \leq n_x + n_h - 2$ , where  $(a, b)$  is given in (22).

$$v_{n_I}[m] = \begin{cases} \sum_{l=0}^m h_I[l]x_{n_I}[m-l] - h_Q[l]x_{n_Q}[m-l] & 0 \leq m \leq n_h - 2, \\ \sum_{l=0}^{n_h-1} h_I[l]x_{n_I}[m-l] - h_Q[l]x_{n_Q}[m-l] & n_h - 1 \leq m \leq n_x - 1, \\ \sum_{l=m-n_x+1}^{n_h-1} h_I[l]x_{n_I}[m-l] - h_Q[l]x_{n_Q}[m-l] & n_x \leq m \leq n_x + n_h - 2, \\ 0 & n_x + n_h - 1 \leq m \leq n_s - 1 \end{cases} \quad (44)$$

The CHF of the random variable  $X \triangleq X_1 + X_2 + \dots + X_L$ , where  $X_i$  and  $X_j$  are independent random variables, is given as follows

$$\phi_X(t) = \phi_{X_1}(t)\phi_{X_2}(t) \dots \phi_{X_L}(t). \quad (48)$$

By employing (48), we can write the random variable  $V_{n_I}[m]$  with the CHF in (47) as the summation of independent random variables as follows

$$V_{n_I}[m] = \sum_{k=a}^b (E_k - E'_k) = V_1 - V_2, \quad (49)$$

where  $V_1 \triangleq \sum_{k=a}^b E_k$ ,  $V_2 \triangleq \sum_{k=a}^b E'_k$ , and  $(a, b)$  is given in (22). In (49),  $E_k$  and  $E'_k$  are independent and exponentially distributed random variables with rate parameter  $\lambda_k = (\sigma_{h_k}\sigma_x/2)^{-1}$ . Using equation (7) in [42], we can write the PDF of  $V_1$  as follows

$$f_{V_1}(v_1) = \prod_{i=a}^b \lambda_i \sum_{j=a}^b \frac{e^{-\lambda_j v_1}}{\prod_{k=a, k \neq j}^b (\lambda_k - \lambda_j)}. \quad (50)$$

Similar expression holds for the PDF of  $V_2$ . Since  $V_{n_I}[m] = V_1 - V_2$ , and  $V_1, V_2 \in [0, \infty)$ , then,  $V_{n_I}[m] \in (-\infty, \infty)$ .

The PDF of the sum of two independent random variables is the convolution of their PDFs. Since  $V_1$  and  $V_2$  are independent random variables, for  $v \geq 0$ , we can write

$$\begin{aligned} f_{V_{n_I}[m]}(v|H_0) &= \int_0^\infty f_{V_1}(v+v_2)f_{V_2}(v_2)dv_2 \\ &= \int_0^\infty \prod_{i=a}^b \lambda_i \sum_{j=a}^b \frac{e^{-\lambda_j(v+v_2)}}{\prod_{k=a, k \neq j}^b (\lambda_k - \lambda_j)} \\ &\quad \times \prod_{r=a}^b \lambda_r \sum_{n=a}^b \frac{e^{-\lambda_n v_2}}{\prod_{p=a, p \neq j}^b (\lambda_p - \lambda_n)} dv_2 \\ &= \left( \prod_{i=a}^b \lambda_i \right)^2 \sum_{j=a}^b \sum_{n=a}^b \frac{1}{\prod_{k=a, k \neq j}^b (\lambda_k - \lambda_j)} \\ &\quad \times \frac{1}{\prod_{p=a, p \neq j}^b (\lambda_p - \lambda_n)} \frac{e^{-\lambda_j v}}{\lambda_j + \lambda_n}. \end{aligned} \quad (51)$$

Similarly, for  $v \leq 0$ , we obtain

$$\begin{aligned} f_{V_{n_I}[m]}(v|H_0) &= \left( \prod_{i=a}^b \lambda_i \right)^2 \sum_{j=a}^b \sum_{n=a}^b \frac{1}{\prod_{k=a, k \neq j}^b (\lambda_k - \lambda_j)} \\ &\quad \times \frac{1}{\prod_{p=a, p \neq j}^b (\lambda_p - \lambda_n)} \frac{e^{\lambda_j v}}{\lambda_j + \lambda_n}. \end{aligned} \quad (52)$$

Now, we can write the PDF of the received sample  $y_{n_I}[m]$  as the convolution of  $f_{V_{n_I}[m]}(v|H_0)$  and  $f_{W_{n_I}[m]}(w|H_0)$  as follows

$$\begin{aligned} f_{Y_{n_I}[m]}(y|H_0) &= \int_{-\infty}^\infty f_{W_{n_I}[m]}(y-v)f_{V_{n_I}[m]}(v|H_0)dv \\ &= \underbrace{\int_0^\infty f_{W_{n_I}[m]}(y-v)f_{V_{n_I}[m]}(v|H_0)dv}_{C_1} \\ &\quad + \underbrace{\int_{-\infty}^0 f_{W_{n_I}[m]}(y-v)f_{V_{n_I}[m]}(v|H_0)dv}_{C_2}. \end{aligned} \quad (53)$$

By using (51) and  $f_{W_{n_I}[m]}(w|H_0) = \mathcal{CN}(0, \sigma_w^2/2)$ , the first integral in (53) can be obtained as follows

$$\begin{aligned} C_1 &= \left( \prod_{i=a}^b \lambda_i \right)^2 \sum_{j=a}^b \sum_{n=a}^b \frac{1}{\prod_{k=a, k \neq j}^b (\lambda_k - \lambda_j)} \frac{1}{(\lambda_j + \lambda_n)\pi\sigma_w^2} \\ &\quad \times \frac{1}{\prod_{p=a, p \neq j}^b (\lambda_p - \lambda_n)} e^{-\frac{y^2}{\sigma_w^2}} \int_0^\infty e^{-\frac{v^2}{\sigma_w^2} - (\lambda_j - \frac{2y}{\sigma_w^2})v} dv \\ &\stackrel{(g)}{=} \left( \prod_{i=a}^b \lambda_i \right)^2 \sum_{j=a}^b \sum_{n=a}^b \frac{e^{(\frac{\lambda_j \sigma_w}{2})^2}}{\prod_{k=a, k \neq j}^b (\lambda_k - \lambda_j)} \frac{1}{2(\lambda_j + \lambda_n)} \\ &\quad \times \frac{1}{\prod_{p=a, p \neq j}^b (\lambda_p - \lambda_n)} e^{-\lambda_j y} \left( 1 - \Phi\left(\frac{\lambda_j \sigma_w}{2} - \frac{y}{\sigma_w}\right) \right), \end{aligned} \quad (54)$$

where (g) comes from [43] (page 336, 3.322, formula 2), and  $\Phi(x) = \text{erf}(x) = \frac{2}{\sqrt{\pi}} \int_0^x e^{-t^2} dt$  denotes the Gaussian error function. Analogous to (54), by using (52) and after some mathematical simplifications, we obtain

$$\begin{aligned} C_2 &= \left( \prod_{i=a}^b \lambda_i \right)^2 \sum_{j=a}^b \sum_{n=a}^b \frac{1}{\prod_{k=a, k \neq j}^b (\lambda_k - \lambda_j)} \\ &\quad \times \frac{1}{\prod_{p=a, p \neq j}^b (\lambda_p - \lambda_n)} \frac{1}{2(\lambda_j + \lambda_n)} \\ &\quad \times e^{\left(\frac{\lambda_j \sigma_w}{2}\right)^2} e^{\lambda_j y} \left( 1 - \Phi\left(\frac{\lambda_j \sigma_w}{2} + \frac{y}{\sigma_w}\right) \right). \end{aligned} \quad (55)$$

Finally, by substituting (54) and (55) into (53), (20) is derived. One can derive an identical expression for the quadrature component of the received samples by following the same procedure.

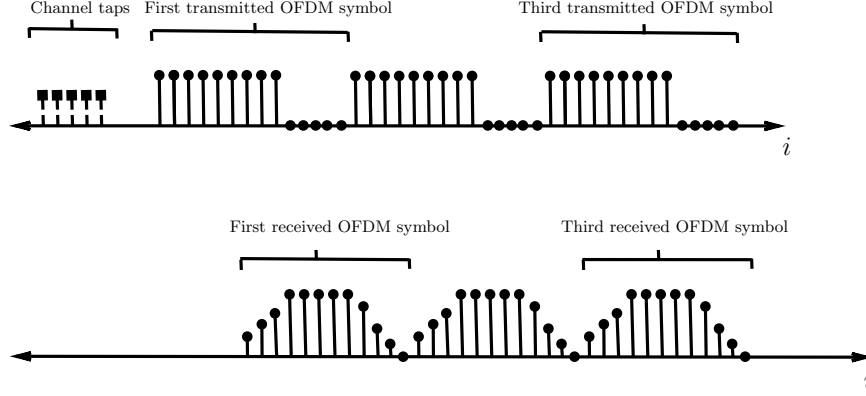


Fig. 11: Convolution of OFDM symbols with a multi-tap channel results in four region given in (44).

### APPENDIX III

In order to perceive the relation between  $f_{Y_n[m]}(y|H_0)$  and  $f_{Y_n[m]}(y|H_d)$ , we rely on the following observations resulting from Theorem 2.

1) For  $n \geq 0$ , there is a repeating pattern in the PDF of the received samples due to the zero-padded guard interval and Gaussianity of the OFDM samples, i.e.,  $x_n(mT_{sa}) \sim \mathcal{CN}(0, \sigma_x^2)$ . Hence, we have

$$f_{Y_{(n+q)I}[m]}(y_I|H_0) = f_{Y_{nI}[m]}(y_I|H_0), \quad q \geq 0, \quad (56)$$

The same equality holds for  $f_{Y_{nQ}[m]}(y_Q|H_0)$ . This repetition pattern is shown in Fig. 11. For simplicity of presentation, we remove the index of the OFDM symbol due to this periodicity and write

$$f_{Y_{nI}[m]}(y_I|H_0) \triangleq f_{Y_I[m]}(y_I|H_0), \quad n \geq 0. \quad (57)$$

The same definition holds for  $f_{Y_{nQ}[m]}(y_Q|H_0)$ . Following the notation in (57), we can write

$$\begin{aligned} f_{Y_n[m]}(y|H_0) &\approx f_{Y_{nI}[m]}(y_I|H_0)f_{Y_{nQ}[m]}(y_Q|H_0) \\ &\triangleq f_{Y_I[m]}(y_I|H_0)f_{Y_Q[m]}(y_Q|H_0) \triangleq \tilde{f}_Y[m](y|H_0). \end{aligned} \quad (58)$$

2) For  $n < 0$ ,  $f_{Y_n[m]}(y|H_0)$  is the PDF of the complex Gaussian noise. For simplicity of presentation, we define

$$\begin{aligned} f_{Y_n[m]}(y|H_0) &\approx f_{Y_{nI}[m]}(y_I|H_0)f_{Y_{nQ}[m]}(y_Q|H_0) \\ &\triangleq f_{Y_{I[-]}[m]}(y_I|H_0)f_{Y_{Q[-]}[m]}(y_Q|H_0) \\ &\triangleq \tilde{f}_{Y[-]}[m](y|H_0), \quad n < 0. \end{aligned} \quad (59)$$

By using (58) and (59), we can define the vector of PDF for the observations vectors  $\{\dots, \mathbf{y}_{-2}^T, \mathbf{y}_{-1}^T, \mathbf{y}_0^T, \mathbf{y}_1^T, \mathbf{y}_2^T, \dots\}$  given hypothesis  $H_0$  as follows

$$\mathbf{f}_Y(\cdot; H_0) \triangleq$$

$$\begin{bmatrix} \vdots \\ f_{Y_{-1}[n_s-2]}(\cdot|H_0) \\ f_{Y_{-1}[n_s-1]}(\cdot|H_0) \\ \vdots \\ f_{Y_0[0]}(\cdot|H_0) \\ f_{Y_0[1]}(\cdot|H_0) \\ \vdots \\ f_{Y_0[n_s-1]}(\cdot|H_0) \\ \vdots \\ f_{Y_1[0]}(\cdot|H_0) \\ f_{Y_1[1]}(\cdot|H_0) \\ \vdots \\ f_{Y_1[n_s-1]}(\cdot|H_0) \\ \vdots \end{bmatrix} = \begin{bmatrix} \vdots \\ \tilde{f}_{Y[-]}[n_s-2](\cdot|H_0) \\ \tilde{f}_{Y[-]}[n_s-1](\cdot|H_0) \\ \vdots \\ \tilde{f}_{Y[0]}(\cdot|H_0) \\ \tilde{f}_{Y[1]}(\cdot|H_0) \\ \vdots \\ \tilde{f}_{Y[n_s-1]}(\cdot|H_0) \\ \vdots \\ \tilde{f}_{Y[0]}(\cdot|H_0) \\ \tilde{f}_{Y[1]}(\cdot|H_0) \\ \vdots \\ \tilde{f}_{Y[n_s-1]}(\cdot|H_0) \\ \vdots \end{bmatrix}. \quad (60)$$

As seen in (60), the right-hand side vector simply represents the repetition pattern of the PDF.

The vector of PDF for the observation vector  $\mathbf{y}$  in (15) given hypothesis  $H_d$  is expressed as follows

$$\mathbf{f}_Y(\mathbf{y}|H_d) = \mathbf{f}_Y^{(d:d+Nn_s-1)}(\mathbf{y}; H_0), \quad (61)$$

where  $\mathbf{f}_Y^{(d:d+Nn_s-1)}(\cdot; H_0)$  is defined in (38). By using (30) and (31), we can write  $\mathbf{f}_Y(\mathbf{y}|H_d)$  in (61) based on  $\tilde{f}_{Y[-]}(\cdot|H_0)$  and  $\tilde{f}_{Y[m]}(\cdot|H_0)$ ,  $m = 0, 1, \dots, n_s - 1$ , as shown in (28) and (29). It is worth mentioning that due to the repetition pattern in  $\mathbf{f}_Y(\cdot; H_0)$ , the truncated PDF vector in (61) contains  $N - 1$  full blocks of  $[\tilde{f}_{Y[0]}(\cdot|H_0), \tilde{f}_{Y[1]}(\cdot|H_0), \dots, \tilde{f}_{Y[n_s-1]}(\cdot|H_0)]^T$ .